frontiers | Frontiers in Earth Science

TYPE Original Research
PUBLISHED 07 June 2023
DOI 10.3389/feart.2023.1199142

OPEN ACCESS

EDITED BY
Liang Chen,
China University of Mining and Technology, China

REVIEWED BY
Wenshuai Li,
Shandong University of Science and Technology, China
Huibin Sun,
Shandong Jianzhu University, China

*CORRESPONDENCE
Chen Cao,
caochen@lntu.edu.cn

RECEIVED 03 April 2023
ACCEPTED 25 May 2023
PUBLISHED 07 June 2023

CITATION
Jia D, Zhi Z, Cao C and Zhang M (2023), Investigations into the failure mechanisms of coal bursts based on a real burst event in the Tangshan coal mine.
Front. Earth Sci. 11:1199142.
doi: 10.3389/feart.2023.1199142

Investigations into the failure mechanisms of coal bursts based on a real burst event in the Tangshan coal mine

Dongxu Jia[1], Zengzhu Zhi[2], Chen Cao[1]* and Ming Zhang[3]

[1]College of Mining, Liaoning Technical University, Fuxin, China, [2]Tangshan Coal Mine, Kailuan (Group) Limited Liability Corporation, Tangshan, China, [3]Research Center of Ministry of Emergency Management, Beijing, China

To investigate the failure mechanisms of coal bursts in the longwalls of underground coal mines, a case study based on the real coal burst in the Tangshan coal mine occurring on 2 August 2019 was carried out to analyze the cause and basic theories of the coal burst and, thus, propose approaches and methods to mitigate the damage. The coal burst occurred mainly due to the sliding of coal from the longwall ribs and the simultaneous uplifting of the floor. As a result of the longwall retraction, the roof above the coal seam was too stable to collapse, forming a long hanging roof behind the longwall. Because the longwall acted as a fulcrum, the hanging roof acted like a saw, exerting massive loads on the longwall. As a result, the roof in front of the longwall tended to slope upward, leaving the underlying coal seam unconfined. Due to the horizontal stresses, the longwall ribs collapsed into the longwall, causing the coal seam to break out. These findings could help improve the fundamental understanding of the failure mechanisms of coal breakouts and, thus, aid in the development of measures to prevent such occurrences.

KEYWORDS

coal burst, mechanical model, roof reflection, normal stress unloading, horizontal ground stress, rib coal slippage

1 Introduction

As mineral resources are depleted at shallow depths, mining depths are increasing by 10–25 m annually, posing further challenges to mining operations (Xie et al., 2015). The high *in situ* stresses, and complex geological and geotechnical conditions in deep earth mining have led to unavoidable bursting events, such as coal bursts in underground coal mines (Lan et al., 2011). Both the frequency and magnitude of burst events have increased significantly. To date, approximately 146 known underground coal mines in China have experienced coal bursts. The database of 2,510 reported coal bursts showed that coal bursts usually occur in the longwall face, longwall face roadways and development roadways, with 86.3% of coal bursts occurring in the longwall face (Tan et al., 2019). Such events usually result in the coal rib entering the roadway, causing damage to mining equipment or even accidents and fatalities. The convergence of the drifts is usually 50%–70% or even up to 90% (Pan, 2018), which causes serious problems for safe mining.

The causes and failure mechanisms of coal burst eruptions are very complex. At first, foreign scientists put forward a series of theories, including the strength theory, the stiffness theory, the energy theory, and the burst proneness theory. Similarly, domestic scholars in

China have also suggested theories. Zang (1987) pointed out that the bursting of coal in the critical state occurs under high stress from mining activities nearby. Qi et al. (2019) proposed a mechanism of frictional sliding failure based on their field observations and tests. Failure during coal bursts may be due to discontinuities between the rock and the coal or weak fills in between. Pan and Zhang (1996) analyzed coal bursts in roadways, longwall faces, and geological structures, and proposed a critical resistance zone theory, in which the ratio of the slope of the stress–strain curve before the peak and after the peak (E/λ) can be used as an important index for the occurrence of coal bursts. Dou et al. (2015) conducted extensive laboratory tests to analyze the strain rate evolution during the testing of coal specimens. They categorized the strain source as static or dynamic and proposed the theory of superimposed static and dynamic strains. Miao et al. (1999) analyzed the yield failure of slab rock at the coal rib and developed a model for crack propagation in the coal rib due to coal excavation. Jiang et al. (2014) proposed an earthquake burst theory for thick coal seams based on case studies of the Yima and Nantun coal mine bursts. Jiang and Zhao (2015) summarized the interactions between the geological structures, *in situ* stresses, and coal outbursts based on the coal outburst in the Yima coal mine in Henan province. Pan (2019) developed a theory for coal eruptions that divided the event into three successive phases, namely, the triggering, energy transfer, and eruption phases.

With the advancement of coal rock fractals, fracture mechanics, loss mechanics, and other rock mechanics, as well as computer science, many domestic and foreign researchers have researched the mechanisms of coal bursts based on these theories. Xie and Pariseau (1993) proposed a fractal theory for coal burst events. Yin et al. (2002) characterized brittle rock using a nonlinear model to develop a model for energy loss during coal burst events. Pan and Yang (2004) conducted extensive laboratory tests and indicated that coal bursts could occur sequentially in the elastic, non-linear, and volumetric expansion phases. Tan et al. (2019) proposed theories of deep mine strain, geologic structural slip, and competent hanging roof bursts based on their field and laboratory test data. Ma et al. (2016) reported that coal bursts in circular roadways would most likely exhibit butterfly-shaped failure in the plastic failure zone and, thus, proposed a "butterfly-shaped failure theory".

As can be seen from the aforementioned discussion, the factors influencing the mechanism of coal bursts are massive and complex. Unfortunately, there remains no conclusive knowledge regarding the causes and failure mechanisms of coal bursts, especially for coal bursts occurring at the coal ribs in the longwall panel roadways. Therefore, this study was mainly a case study based on a real coal burst incident that occurred in the Tangshan coal mine on 2 August 2019. This study aimed to analyze the failure mechanism of the coal burst at the coal rib and propose some measures to prevent the occurrence of such bursts. This study provides a theoretical basis for the prevention and control of this kind of ground impact pressure.

2 General information on the Tangshan coal mine

The Tangshan coal mine is owned by the Kailuan Mining Group. It was built in 1878 and put into operation in 1881, with 145 years of mining activity. The annual production is 3 million tons. The mine is located in the Kailuan mining area, which is on the southeastern side of the Yan Mountain-Southern Foot-Yan Mountain-Sedimentary Rock geological unit. The coal seam is located in the caprock and fold structures in Li County, which were formed by rock alterations in Yan Mountain. The main geological faults in the mining area dip toward NE-SW and run parallel to the ground surface (Yang, 2011). The fault is numbered FI, FII, FIII, FIV, and FV from north to south, with the FV fault in the central and southern areas being the most massive (Jiang et al., 2012). The fold structure dips southward with anticlines and meanwhile dips westward with a series of anticlines. Due to the complexity of the geological structures in the mining area, a series of sub-mining areas have been categorized.

We carried out *in situ* stress measurements at the transport roadways in longwall panel 8,250 and at the bottom of the No. 10 shaft (Table 1). The maximum and minimum main stress inclination angles are close to 0°, corresponding to horizontal stress, while the intermediate principal stress inclination angle is close to 90°, corresponding to vertical stress. The maximum principal stress orientation of each measurement point is between 255.14° and 266.90° in the NEE-SWW direction. The maximum principal stress is between 31.30 MPa and 33.33 Mpa, while the vertical stress *in situ* is between 20.48 Mpa and 22.09 Mpa. The maximum principal stress is about 1.5 times the vertical stress of the overburden.

At present, the main mining areas are in the Yuexu and Nanwu mining districts, with no development and mining activities taking place in other areas. Coal seam Nos. 5, 8, and 9 are mined; in some areas, seam Nos. 8 and 9 are mined at the same time. According to the coal burst susceptibility database, coal seam Nos. 5, 8 and 9 in the Nanwu and Yuexu areas and the coal pillars in the ventilation drift exhibit weak susceptibility to burst, with the roof having weak susceptibility and the floor having weak or no susceptibility.

3 Coal burst incident in the Tangshan coal mine on August 2, 2019

3.1 General information about the area of incident

On August 2, 2019, a massive coal burst occurred at the Tangshan coal mine at the connecting channel of the F5010 ventilation roadway and the crosscut of the F5009 transport roadway (Figure 1). Seven fatalities and five injuries were reported.

Longwall panel F5009 was located on the west side of the field where the coal pillars of the ventilation section were located. The east side of the field was the T_2150 conveyor roadway, and the west side was longwall 3,654. To the south was the potential mining area in F5010 and mining areas T_2155, T_2154, T_2153, and T_2152. To the north were the F5009 coal transport road and the F5009 material transport road. The roadway heights were between 12.6 and 16.6 m. The crosscut in the F5009 material transport roadway was 110 m in length. It was located in the No. 5 seam, and the ceiling was reinforced with rock bolts and a steel arch. The average thickness of the coal seam was 2.6 m, and the average dip angle was 17°. This roadway was developed in June 2017 and referenced with an

TABLE 1 ***In situ*** **stress measurements in the Tangshan coal mine.**

Measurement location	Borehole number	Principal stress category	Principal stress value/MPa	Dip Direction/(°)	Dip angle/(°)
Transport roadway in panel 8,250 (depth: 800.3 m)	1	Maximum σ_1	33.00	259.30	2.01
		Intermediate σ_2	22.09	−18.57	−75.60
		Minimum σ_3	19.60	169.81	−14.25
	2	Maximum σ_1	33.33	264.57	0.86
		Intermediate σ_2	22.19	−1.11	78.76
		Minimum σ_3	21.47	174.40	11.21
Bottom of the No. 10 shaft (depth: 706.2 m)	1	Maximum σ_1	31.73	255.14	2.10
		Intermediate σ_2	20.48	−8.76	70.92
		Minimum σ_3	19.83	164.42	18.95
	2	Maximum σ_1	31.33	256.10	0.53
		Intermediate σ_2	21.22	−12.39	69.72
		Minimum σ_3	20.55	165.99	20.27
	3	Maximum σ_1	31.30	266.90	3.49
		Intermediate σ_2	21.04	4.26	64.54
		Minimum σ_3	20.05	175.26	25.18

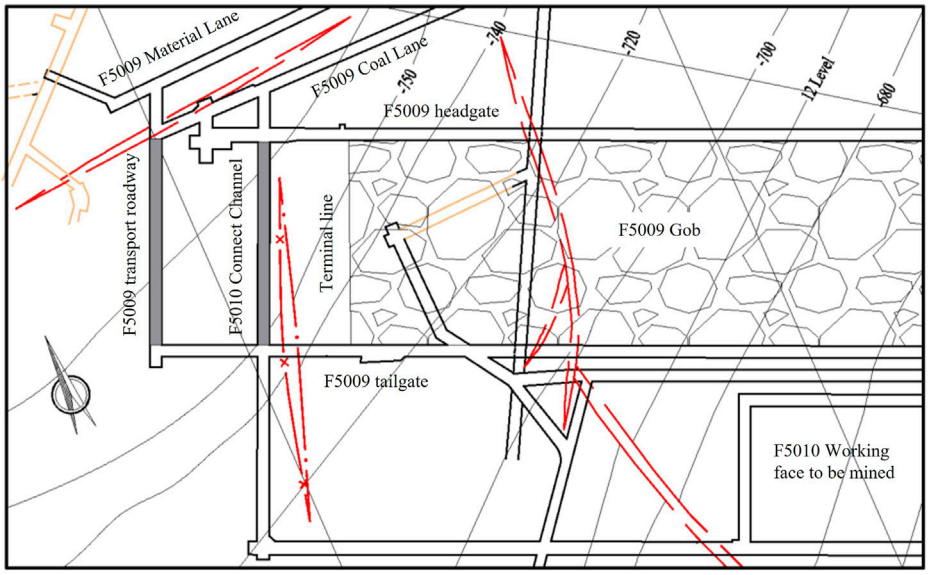

FIGURE 1
Location of the coal burst of "8.2" in the Tangshan coal mine.

elevation of −755.2 m compared to the F5009 wind connection and an elevation of −777.6 m compared to the F5009 transport road connection. It was developed by machinery and drilling and blasting operations.

Longwall field F5010 was located on the west western side of the ventilation shaft coal pillar area. The eastern side of the field was the $T_2$150 conveyor belt route and the western side was the 3654-field mining area. To the south were the $T_2$155, $T_2$154, $T_2$153, and $T_2$152 mining areas. To the north were the mining areas of F5009, the coal transport roadway, and the material transport roadway of F5009. The height of the roadways was between 12.6 and 16.6 m. The connecting channel of F5010 178 m in length and was connected to the ventilation roadway of F5010, the ventilation roadway of F5009, the chain roadway of F5009, and

TABLE 2 Mechanical properties of No. 5 coal seam and its roof.

Rock layer	Rock type	Lithological characteristic	Thickness/m	UCS/MPa
In-direct roof	Slight gray fine sandstone	Composition is mainly quartz and feldspar, siliceous colloid, and has poor sort ability	17.5	143.0
Direct roof	Dark gray fine sandstone	The main components are mainly quartz and feldspar, hard and striped	3.7–6.0	105.1
Fake roof	Sandy mudstone	Muddy composition, siliceous, with fossilized plant leaves	0–0.4	-
No. 5 coal seam	Coal	Black glossy-semi-bright coal, with strip and flake structure, low ash, and low sulfur	2.5	8.5
Direct floor	Sandy mudstone	Composition mud with silica, harder, flat fracture, with plant root fossils	0.4–1.4	-
In-direct floor	White fine sandstone	Main component quartz, banded, siliceous colloidal, with horizontal lamination	5.2	101.3

Note: "-" indicates no relevant data.

the coal transport roadway of F5009. All roadways were secured with rock bolts and steel mesh. The dimensions of the roadways were 4.5 × 3.0 m, and the average inclination angle was 12°. On May 27, roadway support began from the longwall face and extended to the F5010 connecting duct in seam No. 5. On June 18, a support connected to the F5009 ventilation roadway and on July 11 to the F5009 chain roadway. On July 13, a connection was made to the F5009 coal transport roadway and development was complete. The incident occurred in coal seam No. 5, and the roof was sandstone 20-m thick. The UCS of the sandstone was over 100 Mpa. The floor consisted of a combination of sandy mudstone and fine sandstone (Table 2). It is noteworthy that coal seam No. 5 and its blanket showed a weak susceptibility to bursting.

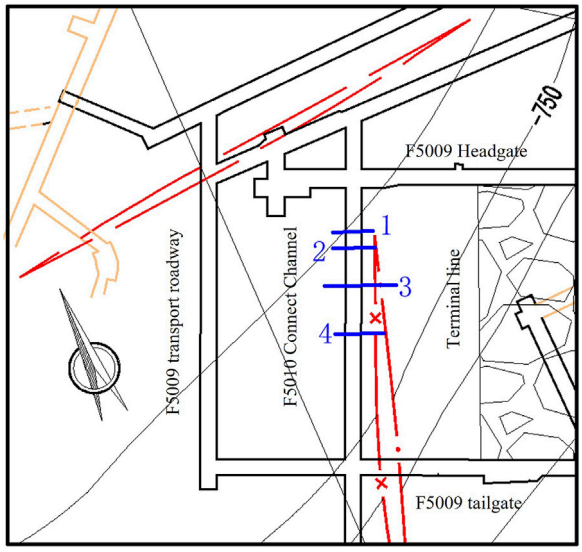

FIGURE 2
Location of the exploration point of the roadway failure.

3.2 Results of the incident investigation

Immediately after the incident, a group of experts was formed. The group conducted extensive research and analysis on the ground and concluded that several causes led to this disaster.

Among these was the complexity of the geological structures and high stresses in the Tangshan coal mine. The accident area was located at the boundary of the FV fault and the stresses in place were very high. The area was also located in the axis zone of the fold syncline and, thus, was subject to a very high local stress concentration. The principal stress was determined to be between 31.30 Mpa and 33.33 Mpa, and the lateral pressure factor constant was between 1.38 and 1.6.

Moreover, the incident area is susceptible to coal bursts. The ceiling and floor of the No. 5 coal seam are weakly susceptible to fracturing. The operating depth in the incident area was nearly 800 m. The weight of the overburden exceeded the UCS of the coal sample. The ceiling of the No. 5 coal seam consisted of hard fine sandstone >20 m in thickness. The UCS of the coal sample was >100 Mpa, and it was reported that the coal tended to accumulate elastic energy.

Additionally, the accident area has a peninsular coal column with high load concentrations. The area was located next to the coal pillar of the ventilation shaft and some mining areas in seam Nos. 5, 8, and 9 in the Tie'er zone. Meanwhile, the F5009 longwall panel also created new mining areas. As a result, there was a superposition of several stresses in the pillar in the area of the incident.

The concentration of stresses induced by mining operations was also high. After the complete retraction of the longwall panel F5009, there was a superposition of stresses in the surrounding roadways, resulting in a high stress concentration. The connecting duct of F5010 is 31 m away from the barrier pillar of F5009, and the coal pillars in the incident area were exposed to a high stress concentration. Moreover, in addition to longwall F5009, the chain and ventilation roadways of F5009 caused further stress concentrations on the coal pillars. Meanwhile, the retrograde mining direction led to the formation of a hanging competent roof, which also transferred massive stresses to the coal pillar. The connecting channel of F5010 and the crosscut of F5009 are oriented perpendicular to the main stress direction, which is unfavorable to the stability of the roadway. A fault 2.5 m high was found to be present at F5009-F6 located 5 m from the connecting channel of F5010. The induced stresses due to the fault structure amplified the stress concentration in the connecting channel of F5010.

Finally, disturbance by development in the roadway also had an effect. A development area in ventilation road 3654E located 80 m from the accident site affected the stability of the rock strata. Mining

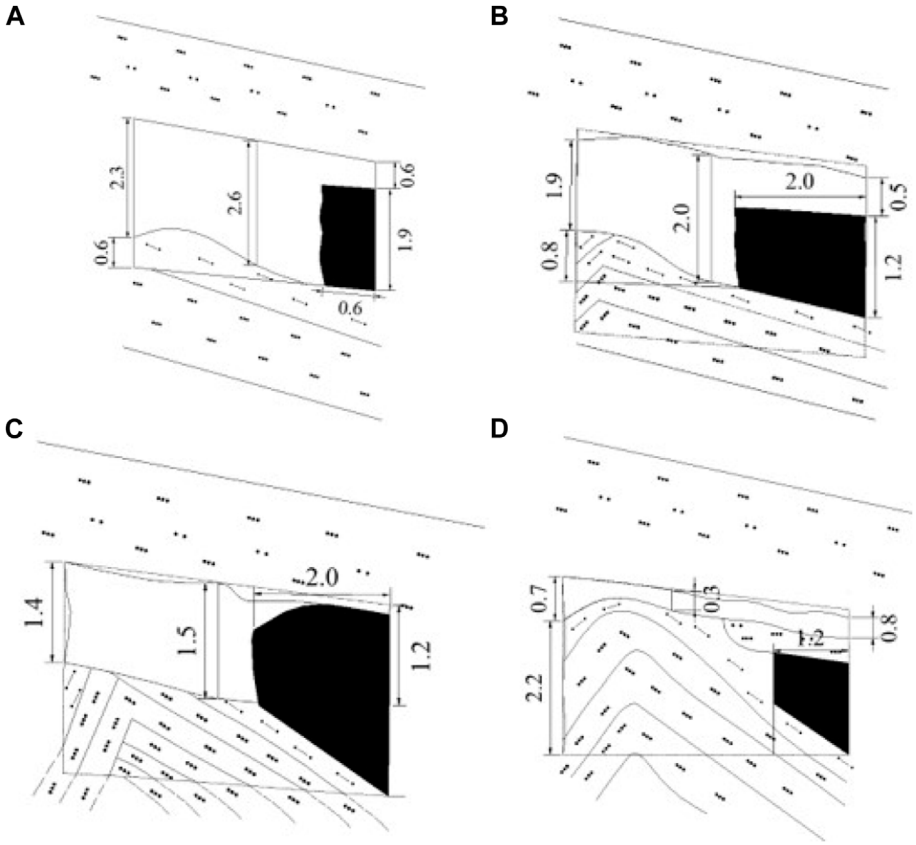

FIGURE 3
Destroy sketch maps for each point of the F5010 connection channel. **(A)** Location 1. **(B)** Location 2. **(C)** Location 3. **(D)** Location 4.

activities in the 3654E roadway also affected the stability of the coal pillars and could have triggered the failure of the pillars.

4 Analysis of the failure mechanism of the incident

4.1 Damage in the underground roadway

The site investigation was conducted in the F5010 connecting channel after the coal burst incident. The locations of all incidents are shown in Figure 2.

The incident occurred at 32.1 m from the lower section of the connecting channel F5010. The roadway is 2.6 m high, and the upper rib is 2.3 m high, while the lower rib is only 0.6 m high. The lower rib has deformed inward by approximately 0.6 m so that the remaining width of the roadway is only 3.5 m. The upper section has a slight ground elevation, as can be seen in Figure 3A.

Another site is located 36.8 m from the lower section of connecting channel F5010. The roadway is 2 m high, and the upper rib is 1.9 m high, while the lower rib is only 0.5 m high. The rib has deformed about 2 m inward. The steel arch for the bottom support has deformed somewhat, as can be seen in Figure 3B.

The third site is 47.2 m from the lower section of connecting channel F5010. The roadway is 1.5 m high, and the upper rib is 1.4 m high. The rib has deformed inward about 2 m so that the roadway is completely closed 1 m from the lower rib (Figure 3C).

The last site is 61.3 m from the lower section of connecting channel F5010. The upper rib is 0.7 m high. The minimum height is 0.3 m and is 1.1 m from the upper rib. The area on the left side of the roadway experienced ground heave, which also resulted in some ground heave on the right side. The rib deformed inward by about 1.2 m, as can be seen in Figure 3D.

As can be seen in Figure 3, the greatest damage and failures occurred at the F5010 connector channel. The roadway was almost completely closed, and there was deformation of the ribs in the roadway and ground elevations.

4.2 Mechanism of coal burst failure

4.2.1 High induced vertical stress in the longwall face

On-site tensions were disturbed by mine development and underground production activities. As a result, the two ribs of the roadway and the longwall were subjected to very high vertical stresses, which were higher than the original stresses on site (Song, 1988).

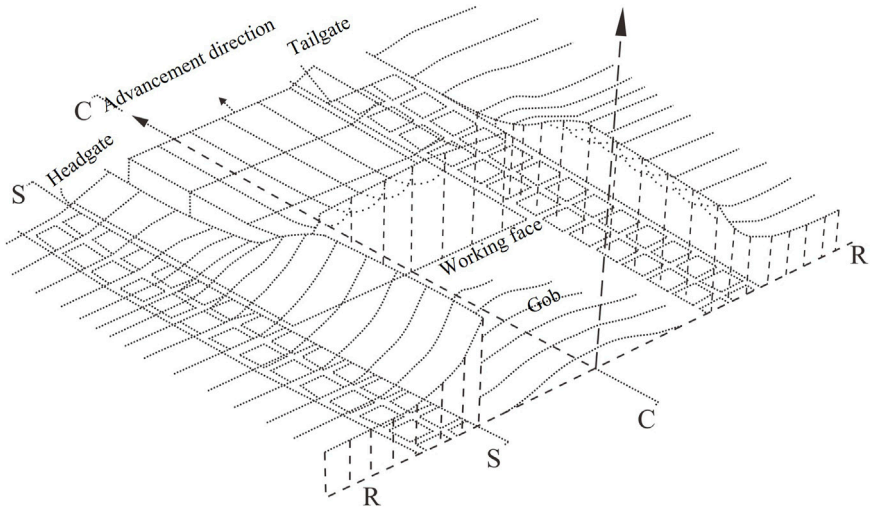

FIGURE 4
Stope abutment pressure distribution.

The vertical stresses originated from different sources. The vertical stresses in the current longwall were mainly carried by the nearby coal seam. The vertical stresses in the adjacent longwall area were carried by the coal pillars. The rib pillars were subjected to the massive vertical stresses emanating from both mining areas. The vertical stresses resulted from the superposition of the two longwall areas, which led to the formation of the maximum vertical stress at the corner of the roadway, as shown in Figure 4.

Vertical stresses depend on the geological conditions of the roof and its mechanical properties. If the roof has a high load-bearing capacity, it will not collapse easily and consequently form a hanging roof. It is worth noting that the rock layers above the hanging roof were also supported by the nearby coal seam. As the longwall moves forward, periodic vertical stress concentration occurs dynamically. This was one of the main causes of the longwall coal burst incident. In this incident, the vertical stresses emanating from the transport roadway and the ventilation roadway overlapped with the vertical stresses in the F5009 longwall, resulting in a massive stress concentration that caused the incident.

4.2.2 High load-carrying capacity of the coal seam

Mining activities led to the formation of massive cavities in the subsurface, causing a disturbance of the stress carried by the coal seam. As a result, stress was removed from at least one direction of the coal seam, resulting in biaxial or even uniaxial stress conditions in the coal seam. Under these complex stress conditions, internal fractures would propagate more easily and lead to ultimate failure. Therefore, four zones were distinguished in the coal seam, namely, the crack zone, the plastic zone, the elastic zone, and the *in situ* zone, from the near field to the far field.

The bearing capacity of the carbon specimen could be significantly improved if the specimen is clamped. Numerous results of true triaxial tests (Gao et al., 2017; Yin et al., 2018; Shen et al., 2019; Lu et al., 2020) confirmed that the maximum compressive strength of the coal specimen increases exponentially with increasing confining pressure. A true triaxial test of four coal specimens was conducted according to the group standard from the Chinese Society of Rock Mechanics & Engineering, titled "Technical specification for true triaxial test of rock specimen (T/CSRME007-2021)". The specimen information and results are shown in Table 3. The densities of the specimens are close to each other, but no significant relationship with their compressive strengths at different confining pressures was observed. As shown in Figure 5, the maximum compressive strengths of the coal specimens at different confining pressures were determined to be 53.08 Mpa, 64.64 Mpa, 82.04 Mpa, and 91.37 Mpa. This indicated that increasing the confining pressure could increase the compressive strength by 21.8%, 54.6%, and 72.1%, respectively.

After a mine is developed and mined, cavities will form. Crack zones, elastic zones, plastic zones, and *in situ* zones will form in the mined areas from the near field to the far field. According to the experience with the paste, the boundary between the elastic zone and the plastic zone is <2 m from the longwall face. This means that the horizontal *in situ* stress is equal to the original stress when the zone is >2 m away from the longwall. In the elastic zone, the bearing capacity of the coal seam increases significantly with increasing rock pressure. Therefore, the zone near the longwall experiences elastic deformation. The vertical deformation depends on the stress in place, the elastic modulus, and the mining height. In such a condition, where the hard and competent coal seam bears high stresses, the coal would tend to burst.

4.2.3 Hanging roof tilt

Since the coal seam in the longwall is competent and could support a massive vertical load from the roof, the immediate roof above the seam would slope upward if the length of the hanging roof is sufficient (Figure 6).

The short black arrow in the figure indicates the direction of gravity of the overlying rock layers, while the long black arrow indicates the vertical load from the hanging roof due to mining activity based on data from field measurements. The coal seam at the longwall is strong enough to support a substantial load. Therefore,

TABLE 3 Results of true triaxial test coal specimens.

Number	Size (length × width × height)/mm	Density/kg·m^{-3}	σ_x/MPa	σ_y/MPa	σ_{zmax}/MPa
M-1	50.43 × 50.58×100.16	1,295	4	2	53.08
M-2	50.13 × 50.19×100.61	1,315	8	4	64.64
M-3	50.25 × 49.68×101.11	1,258	24	12	82.04
M-4	50.85 × 50.62×100.34	1,265	32	16	91.37

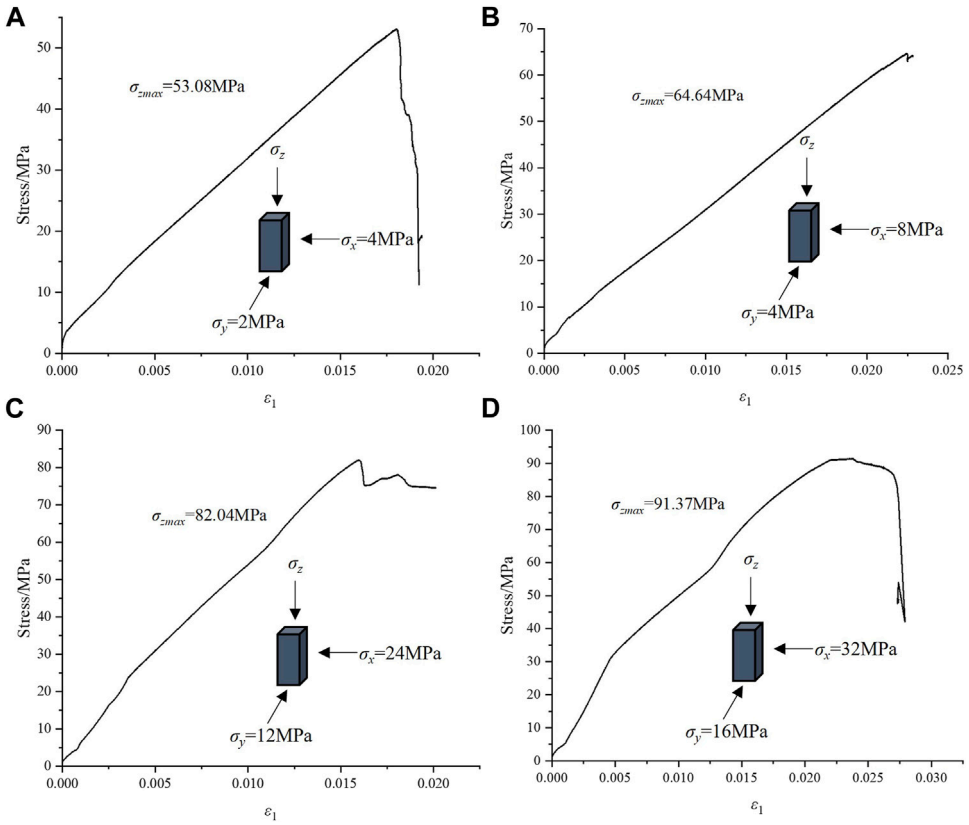

FIGURE 5
earing capacity increases greatly with increased confining pressure. **(A)** M-1. **(B)** M-2. **(C)** M-3. **(D)** M-4.

the roof above the seam would tilt upward if the longwall face moved forward a bit (blue arrow in the figure). The longwall would then act as a fulcrum. The hanging roof behind the longwall face would compress the coal seam at the longwall face, causing the roof above the coal seam in front of the longwall face to straighten.

5 Mitigation measures for coal bursts

5.1 Improvement of the mitigation system

In the Tangshan coal mine, a sophisticated coal burst containment system has been developed in recent years. Coal breakout containment is the most important task in the Tangshan coal mine and, so far, many pieces of high-tech monitoring equipment have been used to monitor the voltage change, the deformation of the roadway, etc. In addition, equipment for stress relief and energy field mapping has also been purchased and implemented. A sophisticated damage mitigation system has been developed and a professional team of technicians has been established.

Based on work experience, a coal outburst mitigation procedure has been developed, which includes 29 coal burst control and mitigation measures. The main principle is to optimize the design so that coal burst incidents are less likely to occur. Then, real-time and field measurements and evaluations must be conducted continuously to prevent incidents. In the meantime, a mature flash relief measure has been developed that can be implemented as soon as a potential coal burst is detected. In addition, upper limits on mining depth, mine production, and

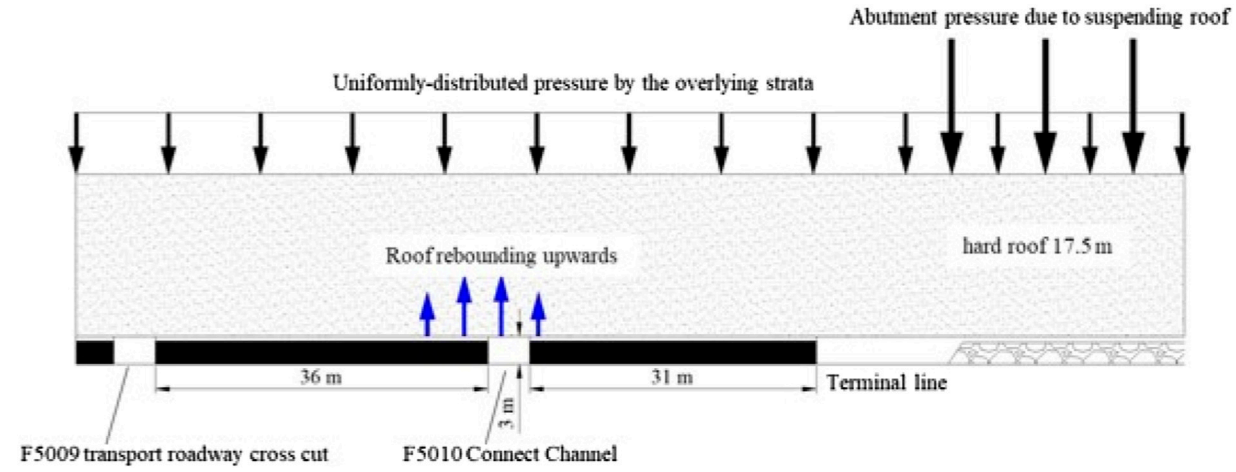

FIGURE 6
Seesaw structure formed by the hard roof and high-bearing coal.

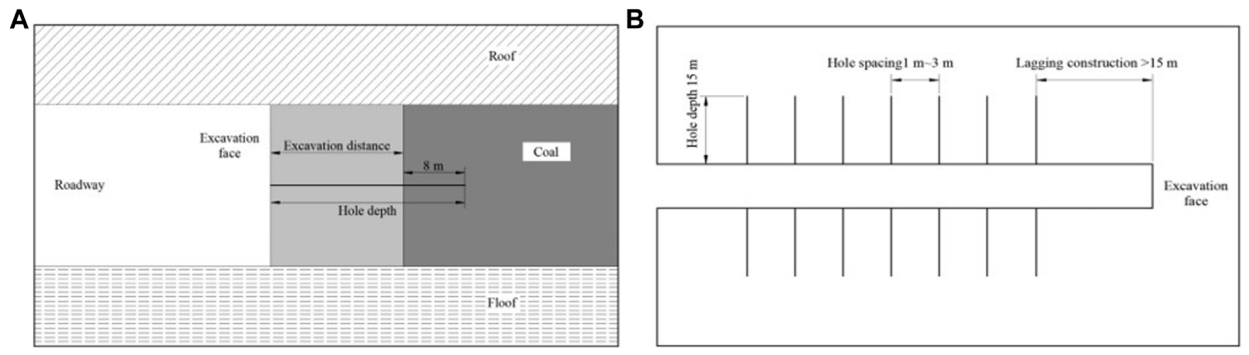

FIGURE 7
Schematic diagram of the pre-pressure relief method. **(A)** Excavation front. **(B)** Excavation rear.

number of underground crews must be established. Attention should also be paid to rock reinforcement and ground support.

A mature early warning system for coal bursts has also been well developed at the Tangshan coal mine. Both local and global seismicity monitoring systems were implemented and are continuously operated by trained technicians. The time and location of each seismic event can be recorded. In addition, the drilling stress-releasing method, real-time stress monitoring, and electromagnetic radiation method are also used to monitor the risk of bursts. In particular, a system was installed to monitor seismicity in the ARAMIS M/E and KJ768 Zones. Three roof deformation monitoring systems were installed in the KJ24 zone. Three acoustic and electrical monitoring systems were installed in the YDD16 Zone and two in the KBD5 Zone. Five trained technicians were assigned to coal excavation mitigation and related risk monitoring only. Four mining engineers were assigned to mitigation activities and are responsible for monitoring data and operating the early warning system. A daily report on the monitoring of the coal burst is prepared and forwarded to the management team.

5.2 Optimization of mitigation measures

5.2.1 Optimization of local mitigation measures

Coal seam nos 5, 8, and 9 are mined simultaneously in the Tangshan coal mine. We propose to give priority to coal seam No. 5 to minimize the risks of coal burst in coal seam nos. 8 and 9. When the mine was designed, the main drift, main development tunnel, and access tunnels were constructed in the rock strata to minimize the risk of a burst. Some mining zones were mined simultaneously, and in one zone, at least one slab was left between two active slabs. In one zone, only one side was mined at a time. Thus, the disturbance of the stress distribution was minimized. The frequency of coal bursts depended on the speed of the longwall movement. The higher the speed, the more energetic events occurred. Therefore, an appropriate mining speed could significantly reduce the risk and frequency of coal bursts.

5.2.2 Optimization of stress-releasing practices

We propose a stress relief method to address the challenges associated with the pivot formed under high stress concentrations.

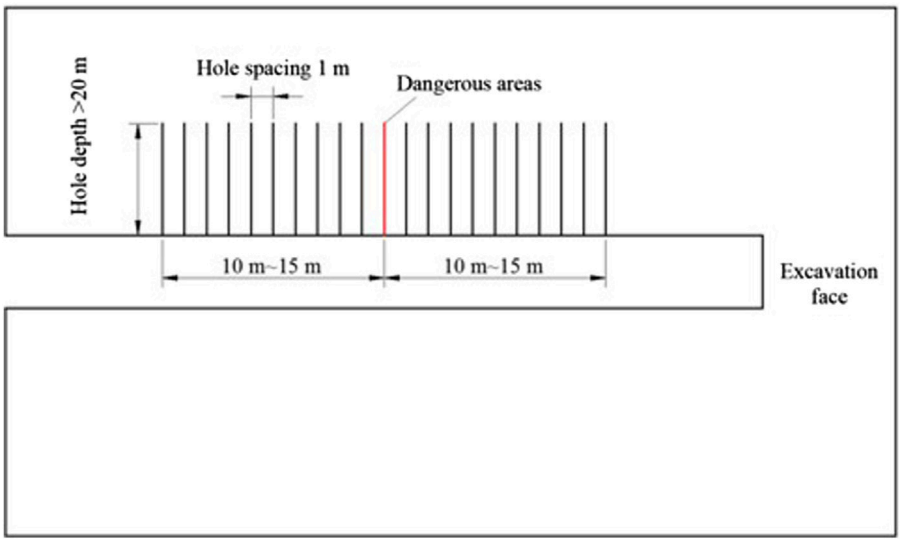

FIGURE 8
Schematic diagram of the pressure relief method.

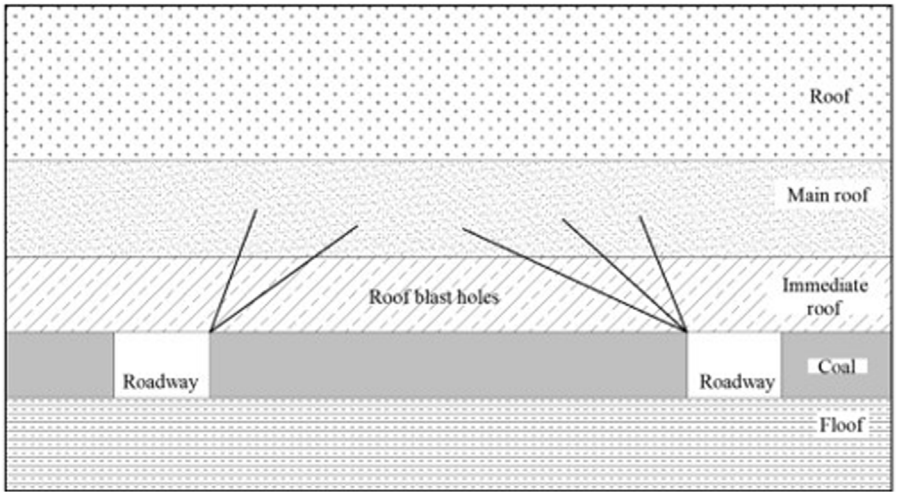

FIGURE 9
Schematic diagram of the roof blasting.

Preconditioning method: the borehole should not be less than 110 mm in diameter. During the development phase, 1–3 holes are drilled, depending on the assessment of coal burst risk, to ensure that stress relief is present in the rock 8 m from the development face (Figure 7A). Behind the mining face, holes should be drilled to a depth of 15 m and no less than 10 m from the mining face. The drill hole spacing should range from 1 to 3 m, depending on the assessment of the risk of a coal burst (Figure 7B). During the longwall retreat phase, 200 m in front of the longwall should be relieved, with an arrangement similar to that in the development stage.

Stress relief method: the borehole should not be less than 110 mm in diameter. In the development stage, the pattern is like a three-petaled flower. The depth of the borehole should exceed 20 m. If there is a risk behind the rock wall, the borehole should be drilled 10–15 m away from the monitoring points. The spacing between boreholes should be 1 m (Figure 8). During the longwall retraction phase, 200 m in front of the longwall should be relieved, with an arrangement similar to that in the development phase.

Considering the formation of a long, hanging roof after the longwall has moved somewhat forward, a method of long-hole drilling and blasting was proposed to relieve the stresses. In the areas at high risk for bursts where blasting was performed, long-hole drilling and blasting significantly relieved the stresses, ensuring a safe environment for subsequent mining activities. A hydraulic drill rig and a special drill bit were used to perform the long-hole drilling with a borehole diameter of no less than 72 mm. Three to five holes

were drilled every 10–15 m in the two roadways adjacent to the longwall (Figure 9). Angled holes were also drilled in the ceiling 1.5 m from the rib. The borehole spacing, angles, and depth could be adjusted depending on site conditions. After the explosives were installed, the drill holes were sealed with mud. The blasting was carried out in accordance with the Safe Mining Regulation.

5.2.3 Stress-relief facilities

Two drilling vehicles (CMS1-12--/22 (model B)), 15 pneumatic drills (ZQJC-200/5), 5 drills (ZQJC-500), 87 hand drills (FIV-HT), and 109 hydraulic support units were used to contain the coal burst. In addition, 400 self-rescuers (ZYJ-M6), 800 protective helmets (ANF-2), and 1000 PPE were available.

As a result of the prudent remedial measures, safe mining activities were carried out in the Y394, 0250, 0291, and Y251 longwall fields, producing ROM 4.45 million tons of coal, resulting in a profit of 276 million Chinese yuan.

6 Conclusion

1) The results of this study showed that coal sliding in the rib area was the main failure mechanism of coal burst in 8.2 incidents. The maximum deformation of the coal rib was up to 2 m, and significant floor heave was also observed near the failure rib.
2) The cause of the coal burst incident was identified. If the immediate roof was too competent, a long, hanging roof would form as the longwall moved forward slightly. This caused the roof above the coal seam in front of the longwall to tilt upward, releasing the confinement of the coal seam.
3) A number of effective measures to mitigate coal bursts have been proposed, with very promising results. The research results provide new ideas for coal outburst prevention and control that can effectively contain the occurrence of similar ground pressure and ensure safe production in mines.

Data availability statement

The original contributions presented in the study are included in the article/Supplementary Material. Further inquiries can be directed to the corresponding author.

Author contributions

DJ was mainly responsible for the overall writing of the full text. ZZ and MZ were responsible for the theoretical analysis. CC was responsible for the innovative ideas in this article. All authors contributed to the article and approved the submitted version.

Conflict of interest

Author ZZ was employed by Tangshan Coal Mine, Kailuan (Group) Limited Liability Corporation. Author MZ was employed by the Research Center of the Ministry of Emergency Management.

The remaining authors declare that the research was conducted in the absence of any commercial or financial relationships that could be construed as a potential conflict of interest.

Publisher's note

All claims expressed in this article are solely those of the authors and do not necessarily represent those of their affiliated organizations, or those of the publisher, the editors, and the reviewers. Any product that may be evaluated in this article, or claim that may be made by its manufacturer, is not guaranteed or endorsed by the publisher.

References

Dou, L., He, J., Cao, A., Gong, S., and Cai, W. (2015). Rock burst prevention methods based on theory of dynamic and static combined load induced in coal mine. *J. China Coal Soc.* 40(7) 469–1476. doi:10.13225/j.cnki.jccs.2014.1815

Gao, Y., Liu, D., Zhang, X., and He, M. (2017). Analysis and optimization of entry stability in underground longwall mining. *Sustainability* 9 (11), 2079. doi:10.3390/su9112079

Jiang, Y., Wang, H., Xue, S., Zhao, Y., Zhu, J., and Pang, X. (2012). Assessment and mitigation of coal bump risk during extraction of an island longwall panel. *Int. J. Coal Geol.* 95, 20–33. doi:10.1016/j.coal.2012.02.003

Jiang, Y., Zhao, Y., Gauthier, A., Baptiste, C., Martinon, P., and Bresse, X. (2015). A comparative public health and budget impact analysis of pneumococcal vaccines: The French case. *Chin. J. Rock Mech. Eng.* 34 (11), 2188–2197. doi:10.1080/21645515.2015.1011957

Jinag, F., Wei, Q., Wang, C., Yao, S., Zhang, Y., Han, R., et al. (2014). Analysis of rock burst mechanism in extra-thick coal seam controlled by huge thick conglomerate and thrust fault. *J. China Coal Soc.* 39 (7), 1191–1196. doi:10.13225/j.cnki.jccs.2013.1402

Lan, H., Qi, Q., Pan, J., and Peng, Y. (2011). Analysis on features as well as prevention and control technology of mine strata pressure bumping in China. *Coal Sci. Tech.* 39 (1), 11–15. doi:10.13199/j.cst.2011.01.17.lanh.008

Lu, J., Yin, G., Gao, H., Li, M., and Deng, B. (2020). Experimental study on compound dynamic disaster and drilling pressure relief of gas-bearing coal under true triaxial loading. *J. China Coal Soc.* 45 (05), 1812–1823. doi:10.13225/j.cnki.jccs.2019.0530

Ma, N., Guo, X., Zhao, Z., Zhao, X., and Liu, H. (2016). Occurrence mechanisms and judging criterion on circular tunnel butterfly rock burst in homogeneous medium. *J. China Coal Soc.* 41 (11), 2679–2688. doi:10.13225/j.cnki.jccs.2016.0788

Miao, X., An, L., Zhai, M., Zhang, X., and Yang, T. (1999). Model of rockburst for extension of slip fracture in palisades. *J. China Univ. Min. Technol.* (2), 15–19.

Pan, J. (2019). Theory of rockburst start-up and its complete technology system. *J. China Coal Soc.* 44 (1), 173–182. doi:10.13225/j.cnki.jccs.2018.1156

Pan, L., and Yang, H. (2004). Dilatancy theory for identification of premonitory information of rock burst. *Chin. J. Rock Mech. Eng.* (S1), 4528–4530. doi:10.3321/j.issn:1000-6915.2004.z1.056

Pan, Y. (2018). *Rock burst in coal mine*. Beijing: Science Press.

Pan, Y., and Zhang, M. (1996). The exact solution for rockburst in coal mine by instability rockburst theory. *Chin. J. Rock Mech. Eng.* S1, 504–510. CNKI:SUN:YSLX.0.1996-S1-017.

Qi, Q., Li, Y., Zhao, S., Zhang, N., and Deng, W. (2019). 70 years development of coal mine rockburst in China: Establishment and consideration of theory and technology system. *Coal Sci. Technol.* 47(9) 1–40. doi:10.13199/j.cnki.cst.2019.09.001

Shen, W., Duo, L., He, H., Gong, S., and Ji, X. (2019). Study on mechanism and prevention of rock burst under loading and unloading path in solid coal driving. *J. Min. Safe. Eng.* 36 (04), 768–776. doi:10.13545/j.cnki.jmse.2019.04.016

Song, Z. (1998). *Practical mine pressure control*. Xuzhou: China university of mining and technology press.

Tan, Y., Guo, W., Xin, H., Zhao, T., Yu, F., and Liu, X. (2019). Key technology of rock burst monitoring and control in deep coal mining. *J. China Coal Soc.* 44 (1), 160–172. doi:10.13225/j.cnki.jccs.2019.5088

Xie, H., Gao, F., and Ju, Y. (2015). Research and development of rock mechanics in deep ground engineering. *Chin. J. Rock Mech. Eng.* 34 (11), 2161–2178. doi:10.13722/j.cnki.jrme.2015.1369

Xie, H., and Pariseau, W. G. (1993). Fractal characteristics and mechanism of rockburst. *Chin. J. Rock Mech. Eng.* (01), 28–37. CNKI:SUN:YSLX.0.1993-01-003.

Yang, Z. (2011). *Investigation on law and prevention technology of coal bump in Kailuan Coal Mine*. [doctoral's Thesis] ([Beijing(China)]: China University of Mining and Technology).

Yin, G., Liu, Y., Li, M., Deng, B., Liu, C., and Lu, J. (2018). Influence of true triaxial loading-unloading stress paths on mechanical property and permeability of coal. *J. China Coal Soc.* 43 (1), 131–136. doi:10.13225/j.cnki.jccs.2017.4500

Yin, G., Zhang, D., Dai, G., and Wang, L. (2022). Damage model of brittle coal and rock burst damage energy index. *J. Chongqing Univ.* (09), 75–78+89. doi:10.3969/j.issn.1000-582X.2002.09.021

Zang, M. (1987). Theory and numerical simulation of rock burst instability. *Chin. J. Rock Mech. Eng.* (3), 197–204. CNKI:SUN:YSLX.0.1987-03-001.